Applied Physics Express

LETTER • OPEN ACCESS

InGaN-based green micro-LED efficiency enhancement by hydrogen passivation of the p-GaN sidewall

To cite this article: Pavel Kirilenko *et al* 2022 *Appl. Phys. Express* **15** 084003

Applied Physics Express 15, 084003 (2022) LETTER
https://doi.org/10.35848/1882-0786/ac7fdc

InGaN-based green micro-LED efficiency enhancement by hydrogen passivation of the p-GaN sidewall

Pavel Kirilenko, Daisuke Iida, Zhe Zhuang, and Kazuhiro Ohkawa*

Electrical and Computer Engineering Program, Computer, Electrical and Mathematical Sciences and Engineering Division, King Abdullah University of Science and Technology (KAUST), Thuwal 23955-6900, Saudi Arabia

*E-mail: kazuhiro.ohkawa@kaust.edu.sa

Received May 24, 2022; revised June 24, 2022; accepted July 7, 2022; published online July 25, 2022

We investigated the effect of the sidewall passivation by hydrogen plasma on the InGaN green micro-LED performance. Hydrogen passivation deactivates the surface region of p-GaN around the perimeter of the device mesa. Thus, hole injection is suppressed in this region, where etching-caused material degradation results in leakage current, decreasing device efficiency. We have confirmed the hydrogen passivation effect on LED square pixels with sizes of 20 and 100 μm. For smaller LEDs, the reverse leakage current has reduced more than tenfold, and the external quantum efficiency of LEDs was enhanced 1.4-times due to the suppression of the non-radiative recombination.

InGaN micro-light-emitting diodes (μLEDs) are widely considered a key technology for the next generation of display realization.[1–3] The display's high resolution is vital for most cutting-edge applications, such as augmented reality and virtual reality wearable devices. Ultra-small ($<10\ \mu$m) LED pixel size is required for high-resolution displays.

The most common method for the III-Nitride LED fabrication is mesa formation using plasma dry etching.[4,5] It was also shown that this method is suitable for the μLED pixel with sub 10 μm size formation.[6–8] Theoretically, with a shrinking device size, the efficiency is supposed to grow due to the better current spreading.[9] However, during the mesa etching, surface damage to the devices' sidewalls is inevitably introduced.[10] With a smaller volume-to-surface ratio, charge carrier diffusion makes carriers' migration into the sidewall region more significant. The sidewall defects induce Shockley–Read–Hall (SRH) non-radiative recombination, resulting in the leakage current.[11] Therefore, with decreasing LED device dimensions, efficiency decreases.[7] Several sidewall treatment techniques have been demonstrated to suppress sidewall damage negative effects, such as wet sidewall wet etching and coating with the passivation layer.[12,13] The wet chemical etching of the LED's sidewall is conventionally carried out by tetramethylammonium hydroxide (TMAH) due to its different etching abilities concerning the different crystallographic planes of GaN.[14] On the other hand, the sidewall passivation layer suppresses any further chemical reactions of the exposed sidewall with air or chemicals involved in further device processing. Materials used as the passivation layer are Al_2O_3,[15,16] SiO_2,[17] HfO_2,[18] ZnO,[19] and AlN.[20]

This work proposes a different approach to overcoming mesa sidewall damage by blocking the current injection into the device's sidewall region. We utilize the phenomenon of p-GaN hydrogen passivation. The Mg dopant atoms in GaN crystal sites bind with hydrogen when exposed to the reactive hydrogen ions. With inactive p-dopant, the exposed p-GaN reportedly increases its sheet resistance by up to 10 times.[21,22] We deliberately expose the LED's sidewalls to the hydrogen plasma while the top surface of the device mesa is coated with a transparent conductive oxide layer, acting here as a hard mask. This procedure results in an insulation layer of passivated p-GaN encircling the LED mesa perimeter. This suppresses current injection into the mesa etching-induced sidewall defects, significantly improving device efficiency.

Commercial InGaN-based green LED wafers were used in this work. The as-received LED structure consisted of a 2 μm thick unintentionally doped GaN, Si-doped n-GaN, 16 periods of InGaN/GaN multiple quantum wells (MQWs), and 300 nm thick Mg-doped p-GaN. Further fabrication was performed to achieve the device structure, as illustrated in Fig. 1. The LED p-side was covered with a 100 nm thick indium-tin-oxide (ITO) layer deposited by the e-beam evaporator, followed by 2-step annealing.[23] Photolithography using a photoresist accompanied by the 100 nm thick SiO_2 hard masks was applied for the mesa formation. The resulting LED pattern consists of square pixel arrays with sizes of $20 \times 20\ \mu m^2$ and $100 \times 100\ \mu m^2$, as shown in Figs. 2(a) and 2(b), respectively. The pixel arrays of $20 \times 20\ \mu m^2$ and $100 \times 100\ \mu m^2$ consisted of 100 pixels and four pixels, respectively. Therefore, in both cases, the effective array area is 4×10^{-4} cm^2.

Dry etching via Cl_2/BCl_3 plasma was performed to achieve 900 nm deep mesa etching, exposing the device n-side. Then, wafers chosen for the hydrogen passivation application were exposed to the hydrogen plasma under the following conditions: radiofrequency plasma generator power 250 W, substrate temperature 300 °C, exposure time 4 min. The top surface of the device p-side, along with the ITO layer, was kept protected by the SiO_2 hard mask. From this point, both wafers with and without application of the hydrogen plasma were processed similarly.

The TMAH wet etching carried out additional sidewall treatment for 40 min at room temperature. Wet etching effectively reduces the sidewall damage.[24] However, in this case, its usage also helps to overcome sidewall contamination by PECVD. Inner surfaces of PECVD chamber, including the carrier wafer, are sputtered with hydrogen plasma and redeposited on the LED chip. TMAH wet etching removes material underneath the contamination, effectively

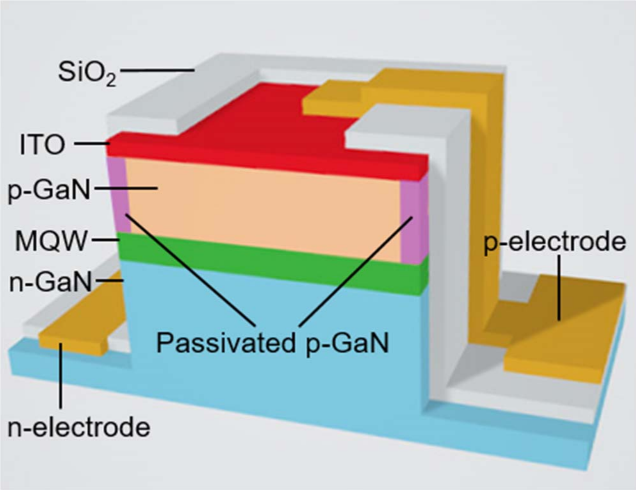

Fig. 1. (Color online) Design schematics for the micro-LED pixel.

removing it as in the lift-off process. Here, we need to keep in mind that TMAH etching is selective to the GaN *m*-plane, with a much lower etch rate along *a*-plane.[14] Choice of the square pixel shape is critical in this case, making the amount of the exposed *a*-plane and *m*-plane sidewalls rotation invariant. After that, the SiO_2 hard mask was removed by wet etching in fluoric acid-based buffered oxide etchant in 7:1 dilution with water for 2 min at room temperature. As illustrated in Fig. 1, the wafer was again covered with a 250 nm thick layer of SiO_2 deposited by plasma-enhanced chemical vapour deposition (PECVD). To expose p- and n-contacts, the SiO_2 layer was selectively removed using C_4F_8 dry plasma etching with patterning realized by photolithography. Both the n-contact and p-pad electrodes consisted of Cr (50 nm)/Pt (195 nm)/Au (200 nm), which were deposited by sputtering.

The device *I*–*V* characteristics and electroluminescence EL performance were characterized using a probe station equipped with an integrating sphere and spectrometer. On-wafer measurements of devices' output power were carried out with an integrating sphere inlet positioned directly above the measured LED at the same height for every device.[25,26] This way, we were able to directly compare devices' output power, wall-plug efficiency (WPE) and external quantum efficiency (EQE). The EL imaging was carried out using an optical microscope.

Figure 3 shows the direct observation of the device EL emission recorded using an optical microscope. Figure 3(a) depicts homogeneous EL along the pixel surface, with typical dark spots. These low-scale inhomogeneities in spatial EL distribution are related to the thermal degradation of InGaN QW[27] and propagating dislocation in LED's active region and p-side.[28,29] The EL observation for the pixel with applied hydrogen passivation, as shown in Fig. 3(b), has a dimmed frame around the pixel perimeter. The drop in the EL intensity in the sidewall region is the direct aftermath of the hydrogen passivation. In the presence of the hydrogen plasma, the Mg dopant atoms at GaN crystal sites are bound with hydrogen ions, decreasing hole concentration. Previous works demonstrated that such a technique could be used to block the current injection into desired parts of the LED.[21,30] That allowed the device pixelation in a frame of a single mesa. Additional measurement was carried out to estimate the merit of the hydrogen ions diffusion depth in the p-GaN.[21] That allowed us to observe the effect of the hydrogen passivation in the p-GaN regions, directly exposed to the hydrogen plasma, and in the thin layer of the masked p-GaN, the so-called hydrogen diffusion region. The width of this region for the plasma exposure conditions, similar to those chosen in the present work, was estimated as 1.7 μm.[21] The width of the dimmed region in Fig. 3(b) agrees with this estimation. Therefore, we can consider that the region of the decreased EL intensity along the LED's pixel perimeter is contributed to the locally suppressed hole injection caused by hydrogen passivation. It is also noticeable that EL emission seems brighter after hydrogen passivation, as shown in Fig. 3. Both microscopy images, (a) and (b), are taken with the same current injection of 10 A cm^{-2}. The increased light power output in the case of the sample with applied hydrogen passivation is confirmed and quantified below. It is important to underline that hydrogen diffusion, in this case, is going in the lateral direction, perpendicular to the *c*-axis of the GaN crystal. Hydrogen diffusion in the p-GaN is slower in the *c*-direction,[31] and with similar plasma exposure conditions, SIMS measurements of hydrogen concentration shows that the diffusion along *c*-axis occurs only in the 100 nm deep layer.

Considering that hydrogen passivation has suppressed injection into the LED regions, severely affected by the dry mesa etching, it is reasonable that the hydrogen passivation effect will be represented in the devices' *I*–*V* behaviour.

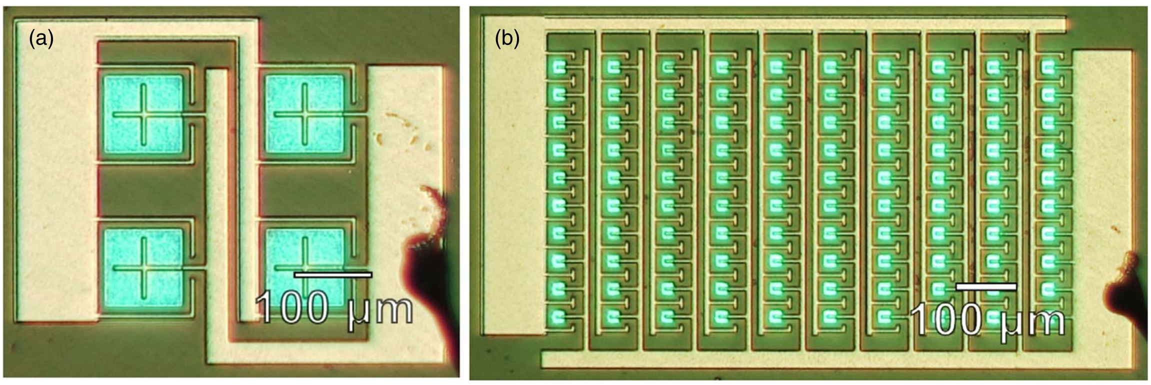

Fig. 2. (Color online) EL images of (a) the 2 × 2 arrays for 100 × 100 μm^2 and (b) the 10 × 10 arrays for 20 × 20 μm^2 μLEDs without hydrogen passivation at 10 A cm^{-2} current injection density under external illumination.

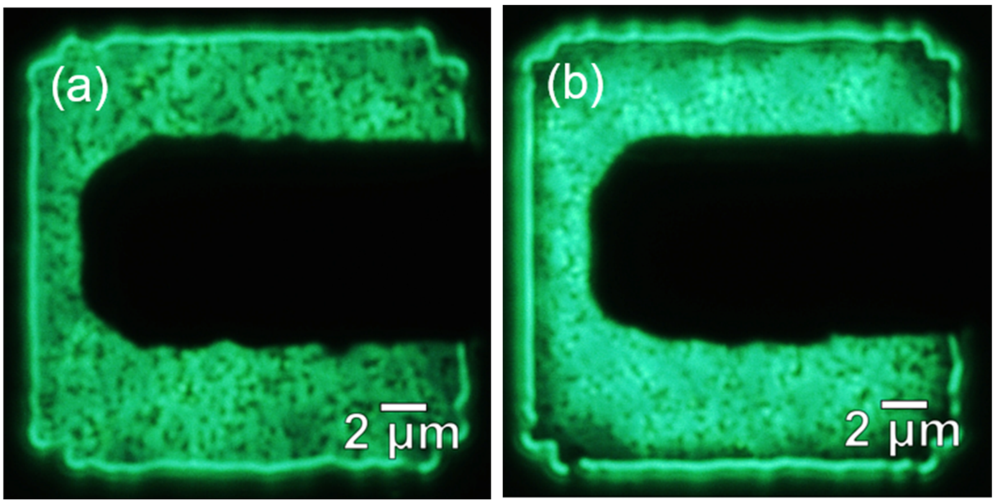

Fig. 3. (Color online) EL images of $20 \times 20\ \mu m^2$ LED pixel under injection current density of 10 A cm^{-2} for (a) reference sample (b) with hydrogen passivation applied.

Keeping in mind that the hydrogen passivation has reduced the effective area of the devices, we have renormalized the current density for the passivated LED chips. Using the fact that diffused hydrogen atom concentration decreases from the surface as a complementary error function[32] and knowing the diffusion length, we calculated the effective area as 95% and 77% of the original device in case of $100 \times 100\ \mu m^2 \times$ 4-chips and $20 \times 20\ \mu m^2 \times$ 100-chips LED arrays, respectively. *I–V* curves of the device arrays of different sizes with and without hydrogen passivation are shown in Fig. 4. Negative currents are given at absolute values to be viewed on a logarithmic scale. For a given LED with an electroluminescence peak at approximately 530 nm, forward voltage V_F is approximately 2.3 V. We can divide represented voltage range (–5 to 5 V) effectively into three regions: (–5 to 0 V)—a region I; (0 to 2.3 V)—region II; (2.3 to 5 V)—region III. It is noticeable that at 2.3 V, the *I–V* curves of all four measured LEDs intersect at one point. It illustrates that the value of V_F is independent of the device fabrication and determined solely by the LED structure. For region I, the positive effect of the hydrogen passivation comes as suppression of the reverse current density. For the reverse bias of –5 V applied, the passing current has reduced 13.4 times and 8.1 times for $100 \times 100\ \mu m^2 \times$ 4-chips and $20 \times 20\ \mu m^2 \times$ 100-chips LED arrays, respectively. A different reverse current for the arrays with different sizes is given by the different total sidewall lengths. In region II, the device is still operating with the closed diode, and its *I–V* behaviour is determined by leakage current, so overall tendencies are the same as those for region I. In region III, the introduction of hydrogen passivation resulted in similar *I–V* behaviours of the arrays of different sizes, which were sufficiently different without hydrogen passivation. That means that the effect of varying device surface-to-perimeter ratios is suppressed, making it easier to reduce device dimensions in future display engineering. Exposure to the hydrogen plasma also reduces device differential resistance in area III. This can contribute to the positive effect of the hydrogen plasma exposure on the n-GaN. Surface defects on the device's n-side caused by dry etching can be passivated by hydrogen termination,[33] improving the quality of the n-contact. We can quantify it by comparing the voltage drop across the device with the selected injection current density. The results are presented in Table I. The most significant reduction in the voltage drop is recorded as 1.85 times in the case of the high injection current density of 25 A cm^{-2} for the $20 \times 20\ \mu m^2 \times$ 100-chips LEDs array.

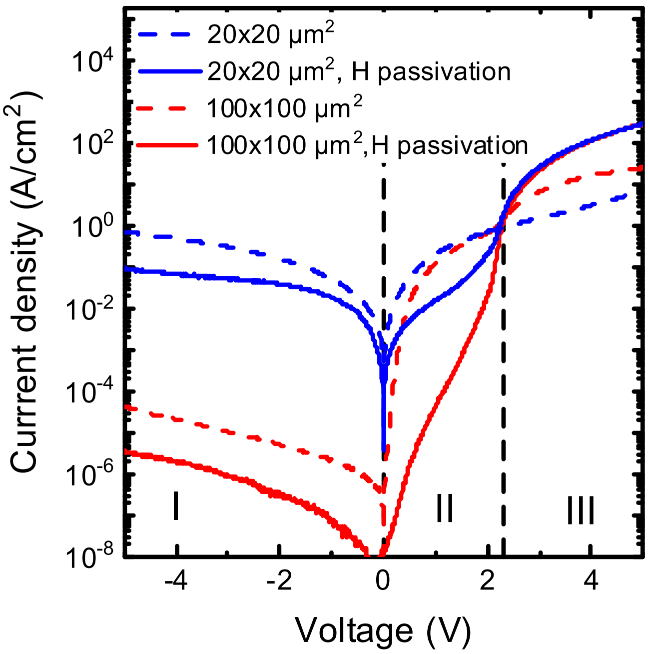

Fig. 4. (Color online) *I–V* characteristics of μLED arrays under forward and reverse bias.

Reduction of the non-radiative recombination by the hydrogen passivation positively impacted the devices' light output power. As shown in Fig. 5(a), at 25 A cm^{-2} forward

Table I. Voltage drop for different current injection density.

Sample	Voltage, V 10 A cm^{-2}	20 A cm^{-2}	25 A cm^{-2}
20 × 20 array, reference	4, 16	5, 13	5, 49
20 × 20 array, H passivation	2, 63	2.87	2.96
100 × 100 array, reference	3, 34	4, 38	4, 91
100 × 100 array, H passivation	2, 7	2, 94	3, 03

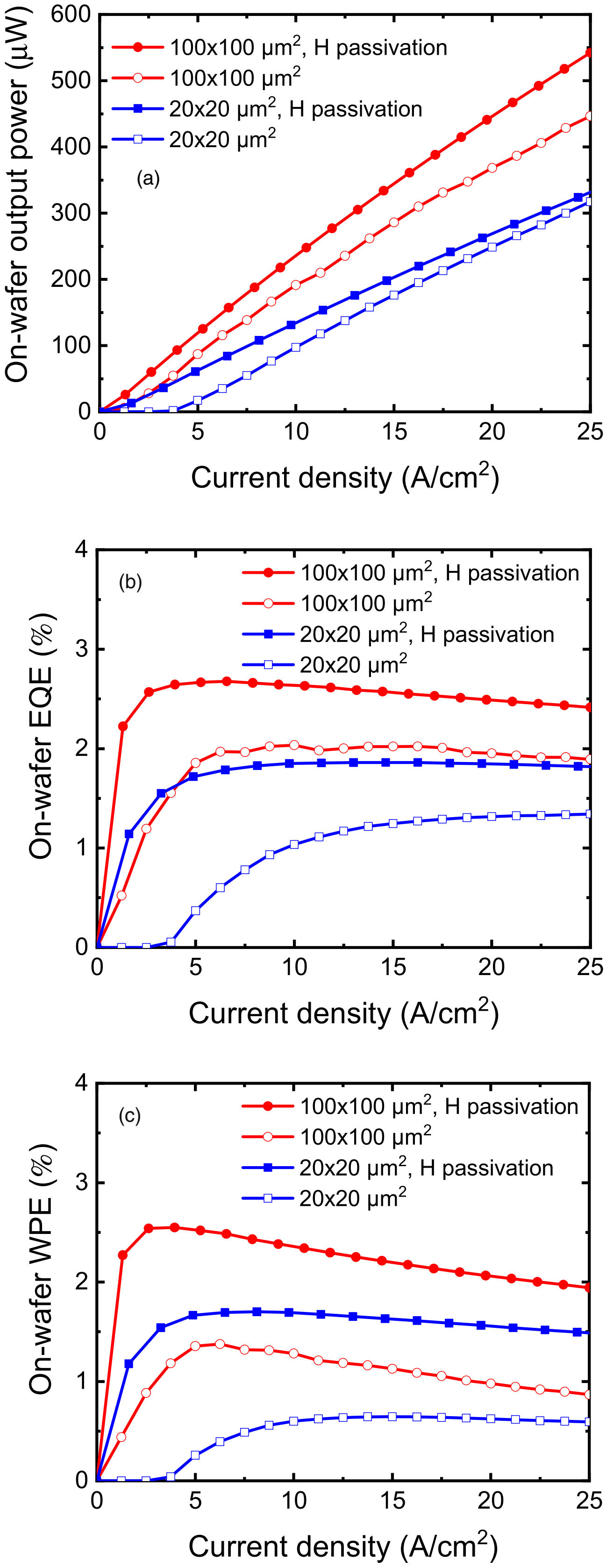

Fig. 5. (Color online) (a) On-wafer output power of μLED arrays versus injection current density, (b) on-wafer EQEs, and (c) on-wafer WPEs of μLED arrays.

current injection density, the $20 \times 20\ \mu m^2 \times 100$-chips LEDs array has shown the light output of 331 μW and 317 μW with and without hydrogen passivation, respectively, which means 5% of output power improvement. In the case of the $100 \times 100\ \mu m^2 \times 4$-chips arrays, those numbers are 542 μW, 447 μW, and 21.2%, respectively. The more minor effect of the hydrogen passivation on the $100 \times 100\ \mu m^2$ pixel size results from a smaller volume-to-surface ratio. It is represented via different perimeter lengths, 8 mm in case of the $20 \times 20\ \mu m^2 \times 100$-chips arrays versus 1.6 mm in case of the $100 \times 100\ \mu m^2 \times 4$-chips arrays with equal device active area of 4×10^{-4} cm^2.

Along with increasing output power, LEDs' EQE improves after introducing the hydrogen passivation. As shown in Fig. 5(b), the EQE peak value has risen from 1.34% to 1.86% and from 2.03% to 2.67% in the case of $20 \times 20\ \mu m^2 \times 100$-chips and $100 \times 100\ \mu m^2 \times 4$-chips LED arrays, respectively. Therefore, LED's EQE has increased 1.4 times in the case of a $20 \times 20\ \mu m^2 \times 100$-chips array and 1.3 times in the case of a $100 \times 100\ \mu m^2 \times 4$-chips array.

We can also observe a shift in the peak EQE position concerning the current injection density. In these terms, the EQE peak has shifted from over 25 A cm^{-2} to 14.6 A cm^{-2} in the case of a $20 \times 20\ \mu m^2 \times 100$-chips array and from 10 A cm^{-2} to 6.6 A cm^{-2} in the case of a $100 \times 100\ \mu m^2 \times 4$-chips array, before and after hydrogen passivation, respectively. LED efficiency improvement, specifically in the low-current region, is caused by a reduction in SRH non-radiative recombination.[34] Efficiency peak position shift with changing device size is caused mainly by this effect.[35] Hydrogen passivation plasma further suppresses SRH non-radiative recombination, reducing the impact of the device's decreasing surface-to-perimeter ratio.

We can outline an improvement in the LEDs' performance by the hydrogen passivation by calculating their WPE in dependence from injection current density. With a simultaneous EQE increase and the lower voltage drop across the device, LEDs' overall WPE increases drastically with the introduction of hydrogen passivation. As shown in Fig. 5(c), the WPE peak value has increased from 0.64% to 1.7% and from 1.38% to 2.55% in the case of $20 \times 20\ \mu m^2 \times 100$-chips and $100 \times 100\ \mu m^2 \times 4$-chips LED arrays, respectively. Therefore, LED's WPE has increased 2.6 times in the case of $20 \times 20\ \mu m^2 \times 100$-chips array and 1.8 times in the case of $100 \times 100\ \mu m^2 \times 4$-chips array. A sufficient increase in device efficiency, especially in the case of smaller LED pixels, makes the hydrogen passivation of p-GaN sidewalls a promising technology for μLED display application.

In this work, we demonstrated the efficiency enhancement of the InGaN μLEDs by hydrogen passivation. We have shown a convenient way to increase LED EQE and WPE. The technology does not require additional photolithography patterning, and the process can be carried out in any PE/PECVD chamber equipped with a hydrogen source and RF plasma generator. Overall, reduction of the non-radiative recombination intensity positively impacts the device lifetime. The devices' WPE has been shown to increase up to 2.6 times. This is a promising technique for fabricating efficient micro-LED chips and displays.

Acknowledgments This work was financially supported by King Abdullah University of Science and Technology (KAUST) (BAS/1/1676-01-01).

ORCID iDs Pavel Kirilenko https://orcid.org/0000-0002-8430-1366 Daisuke Iida https://orcid.org/0000-0002-5385-6238 Zhe Zhuang https://orcid.org/0000-0002-2565-5500 Kazuhiro Ohkawa https://orcid.org/0000-0002-8728-3503

1) M. S. Wong, S. Nakamura, and S. P. DenBaars, ECS J. Solid State Sci. Technol. **9**, 015012 (2019).
2) Z. Y. Fan, J. Y. Lin, and H. X. Jiang, J. Phys. D: Appl. Phys. **41**, 094001 (2008).
3) K. Ding, V. Avrutin, N. Izyumskaya, Ü. Özgür, and H. Morkoç, Appl. Sci. **9**, 1206 (2019).
4) Z. Zhuang, D. Iida, and K. Ohkawa, Appl. Phys. Lett. **116**, 173501 (2020).
5) H. Yu, M. H. Memon, D. Wang, Z. Ren, H. Zhang, C. Huang, M. Tian, H. Sun, and S. Long, Opt. Lett. **46**, 3271 (2021).
6) D. Hwang, A. Mughal, C. D. Pynn, S. Nakamura, and S. P. DenBaars, Appl. Phys. Express **10**, 032101 (2017).
7) J. M. Smith, R. Ley, M. S. Wong, Y. H. Baek, J. H. Kang, C. H. Kim, M. J. Gordon, S. Nakamura, J. S. Speck, and S. P. DenBaars, Appl. Phys. Lett. **116**, 071102 (2020).
8) S. S. Pasayat et al., Appl. Phys. Lett. **117**, 061105 (2020).
9) J. Kou, C.-C. Shen, H. Shao, J. Che, X. Hou, C. Chu, K. Tian, Y. Zhang, Z.-H. Zhang, and H.-C. Kuo, Opt. Express **27**, A643 (2019).
10) J.-H. Park, M. Pristovsek, W. Cai, H. Cheong, T. Kumabe, D.-S. Lee, T.-Y. Seong, and H. Amano, Opt. Lett. **47**, 2250 (2022).
11) K. A. Bulashevich and S. Y. Karpov, Physica Status Solidi (RRL) **10**, 480 (2016).
12) J. Yu et al., Crystals **11**, 403 (2021).
13) M. S. Wong, D. Hwang, A. I. Alhassan, C. Lee, R. Ley, S. Nakamura, and S. P. DenBaars, Opt. Express **26**, 21324 (2018).
14) H. Wan, B. Tang, L. Ning, S. Zhou, C. Gui, and S. Liu, Nanomaterials. **9**, 365 (2019).
15) H.-Y. Liu, W.-C. Hsu, B.-Y. Chou, Y.-H. Wang, W. Sun, S.-Y. Wei, and Y. Shengmin, Photonics Technol. Lett. IEEE. **26**, 1243 (2014).
16) S.-J. So and C.-B. Park, Thin Solid Films **516**, 2031 (2008).
17) H.-H. Huang et al., Opt. Express **28**, 38184 (2020).
18) M. Patel, B. Jain, R. T. Velpula, and H. P. T. Nguyen, ECS Trans. **102**, 35 (2021).
19) Y.-L. Wang, H. S. Kim, D. P. Norton, S. J. Pearton, and F. Ren, Appl. Phys. Lett. **92**, 112101 (2008).
20) D. Chen, Z. Wang, F.-C. Hu, C. Shen, N. Chi, W. Liu, D. W. Zhang, and H.-L. Lu, Opt. Express **29**, 36559 (2021).
21) Z. Zhuang, D. Iida, M. Velazquez-Rizo, and K. Ohkawa, Opt. Lett. **46**, 5092 (2021).
22) A. Y. Polyakov, N. B. Smirnov, A. V. Govorkov, K. H. Baik, S. J. Pearton, B. Luo, F. Ren, and J. M. Zavada, J. Appl. Phys. **94**, 3960 (2003).
23) Z. Zhuang, D. Iida, P. Kirilenko, M. Velazquez-Rizo, and K. Ohkawa, Opt. Express **28**, 12311 (2020).
24) Y. Yang and X. A. Cao, J. Vac. Sci. Technol. B **27**, 2337 (2009).
25) Z. Zhuang, D. Iida, M. Velazquez-Rizo, and K. Ohkawa, IEEE Electron Device Lett. **42**, 1029 (2021).
26) Z. Zhuang, D. Iida, and K. Ohkawa, Jpn. J. Appl. Phys. **61**, SA0809 (2021).
27) Z. Li et al., Appl. Phys. Lett. **103**, 152109 (2013).
28) R. Xia, I. Harrison, E. Larkins, A. Andrianov, S. Dods, J. Morgan, P. Parbrook, C. Button, and G. Hill, Mater. Sci. Eng. B **93**, 234 (2002).
29) L. van Deurzen, M. Ruiz, K. Lee, H. Turski, S. Bharadwaj, R. Page, V. Protasenko, H. Xing, J. Lähnemann, and D. Jena, J. Phys. D: Appl. Phys. **54**, 495106 (2021).
30) Z. Zhuang, D. Iida, and K. Ohkawa, Photon. Res. **9**, 2429 (2021).
31) C. H. Seager, S. M. Myers, A. F. Wright, D. D. Koleske, and A. A. Allerman, J. Appl. Phys. **92**, 7246 (2002).
32) D. Shaw, in *Springer Handbook of Electronic and Photonic Materials*, ed. S. Kasap and P. Capper, (Springer, Berlin, 2017) 2nd ed., p. 121 .
33) S. Chen, K. Ishikawa, Y. Lu, R. Kometani, H. Kondo, Y. Tokuda, T. Egawa, H. Amano, M. Sekine, and M. Hori, Jpn. J. Appl. Phys. **51**, 111002 (2012).
34) J. Piprek, Physica Status Solidi (a) **207**, 2217 (2010).
35) P.-W. Chen, P.-W. Hsiao, H.-J. Chen, B.-S. Lee, K.-P. Chang, C.-C. Yen, R.-H. Horng, and D.-S. Wuu, Sci. Rep. **11**, 22788 (2021).